# *Contribution of tropical cyclones to atmospheric moisture transport and rainfall over East Asia*

# Contribution of Tropical Cyclones to Atmospheric Moisture Transport and Rainfall over East Asia

LIANG GUO, NICHOLAS P. KLINGAMAN, PIER LUIGI VIDALE, ANDREW G. TURNER, AND MARIE-ESTELLE DEMORY

*National Centre for Atmospheric Science, Department of Meteorology, University of Reading, Reading, United Kingdom*

ALISON COBB

*Department of Physics, Imperial College, London, United Kingdom*

(Manuscript received 13 April 2016, in final form 17 January 2017)

ABSTRACT

The coastal region of East Asia (EA) is one of the regions with the most frequent impacts from tropical cyclones (TCs). In this study, rainfall and moisture transports related to TCs are measured over EA, and the contribution of TCs to the regional water budget is compared with other contributors, especially the mean circulation of the EA summer monsoon (EASM). Based on ERA-Interim reanalysis (1979–2012), the trajectories of TCs are identified using an objective feature tracking method. Over 60% of TCs occur from July to October (JASO). During JASO, TC rainfall contributes 10%–30% of the monthly total rainfall over the coastal region of EA; this contribution is highest over the south/southeast coast of China in September. TCs make a larger contribution to daily extreme rainfall (above the 95th percentile): 50%–60% over the EA coast and as high as 70% over Taiwan Island. Compared with the mean EASM, TCs transport less moisture over EA. However, as the peak of the mean seasonal cycle of TCs lags two months behind that of the EASM, the moisture transported by TCs is an important source for the water budget over the EA region when the EASM withdraws. This moisture transport is largely performed by westward-moving TCs. These results improve understanding of the water cycle of EA and provide a useful test bed for evaluating and improving seasonal forecasts and coupled climate models.

## 1. Introduction

East Asia (EA) is affected by one of the most intense monsoon systems; its rainfall and water budget are dominated by the East Asia summer monsoon (EASM). Meanwhile, the western North Pacific (WNP) basin and the coast of EA are regions that have the most frequent impacts from tropical cyclones (TCs). Landfall of TCs is accompanied by destructive winds, storm surges, and heavy rainfall that threaten the lives and socioeconomic systems of hundreds of millions of people living along the EA coast. Forming over the western Pacific warm pool, TCs that move across the EA region bring warm and moist air into land. TCs, therefore, could be a key contributor to the rainfall and water budget over EA, especially over China. Quantifying these contributions of TCs would improve understanding and prediction of water cycle variability over EA, which is essential to agriculture and the local economy.

TC variability has been extensively studied on a variety of temporal scales. Over the WNP and EA regions, studies have covered scales from intraseasonal to decadal. TC variability has been linked with the Madden–Julian oscillation (Feng et al. 2013; Kim et al. 2008; Camargo et al. 2007b), El Niño–Southern Oscillation (Chan 2000; Wang and Chan 2002; Chia and Ropelewski 2002; Camargo et al. 2007a), quasi-biennial oscillation (Ho et al. 2009), and Pacific decadal oscillation (Lee et al. 2012). In general, there are several key aspects of the background state and large-scale circulation over EA that have been linked to TCs on different temporal scales, including sea surface temperature (SST), vertical wind shear, and the positions and intensities of the monsoon trough/intertropical convergence zone (ITCZ) and the western North Pacific subtropical high (WNPSH).

*Corresponding author e-mail*: Liang Guo, l.guo@reading.ac.uk

DOI: 10.1175/JCLI-D-16-0308.1

While the drivers of TC variations over EA have been widely studied, the contributions of TCs to the EA water cycle have received less attention, even in terms of their climatologies. Contributions of TCs to total and extreme rainfall over EA have been investigated using gauge data (Chen et al. 2010, 2012; Ren et al. 2002, 2006; Wu et al. 2007; Wang and Chen 2008). A typical contribution of TCs to the total annual rainfall along the southeastern coastal region is 20%–40%, with the largest impact over Hainan Island off the south China coast (Ren et al. 2006; Wu et al. 2007). During the second half of the twentieth century, the number of TCs affecting China showed a downward trend, accompanied by a decreasing trend in the contribution of TC rainfall to the total rainfall (Ren et al. 2006). Over Taiwan Island, TC rainfall accounts for 40% of total rainfall during late summer to early autumn (Wang and Chen 2008). Over other TC-active regions, the contribution of TC rainfall to the total rainfall varies; however, along the coastal regions, the TC rainfall contribution is 10%–40% (Prat and Nelson 2013; Dare et al. 2012; Prat and Nelson 2016). The contribution of TCs to Australian extreme rainfall and to United States flooding has been analyzed by Villarini and Denniston (2015) and Villarini et al. (2014). Over Australia, more than half of the highest annual rainfall events associated with TCs are over the coastal regions and in particular in western Australia (Villarini and Denniston 2015). TC rainfall accounts for 20%–40% of total rainfall over northwest Australia during the Southern Hemisphere warm season (Dare et al. 2012). TC rainfall is also a major cause of floods in the eastern United States (Villarini et al. 2014). About 14% of total onshore flux over the coast of the North America can be attributed to the Atlantic TCs (Xu et al. 2016).

The aforementioned studies suggest that TCs have the potential to make a substantial contribution to the water cycle over EA. The fact that TC contributions to the atmospheric moisture budget have received little attention may be explained by the perceived dominance of the EASM, one of the most intense monsoon systems on the planet. The water budget is thus dominated by the EASM, which explains why most studies have been concentrating on this aspect, while the role played by TCs in the water cycle has been neglected. This study is therefore an attempt to the gap between studies of the impact of TCs on rainfall and those of the role of the EASM in the moisture budget. As our study will show, because of differences in the timing of the seasonal cycles of TCs and the EASM, the contribution of TCs to the water cycle is nonnegligible, even compared to the substantial transport by the EASM, and is particularly important to EA during the EASM withdrawal phase.

In this study, we decompose the total rainfall and moisture transport into contributions from TCs and from the mean flow. Then, we calculate the contributions of TCs to the rainfall and water budgets and compare these with the EASM in terms of climatology. Data and methods are introduced in section 2; the statistics of TCs over EA are shown in section 3; TC contributions to both total and extreme rainfall are discussed in section 4; and the comparison of moisture transport from TCs with that from the EASM is shown in section 5. Finally, the conclusion and discussion are given in section 6.

## 2. Data and methods

### a. Observation and reanalysis data

To evaluate the contribution of TCs to rainfall over EA, we use the satellite-derived Tropical Rainfall Measuring Mission (TRMM) 3B42 version 7 (v7) rainfall analysis (Huffman and Bolvin 2012), a 3-hourly $0.25° \times 0.25°$ gridded rainfall dataset produced from 1998 onward. The spatial coverage is 50°S–50°N, 180°W–180°E. Chen et al. (2013) showed that TRMM 3B42 v7 has improved skill at detecting intense TC rainfall, with good correlations and spatial patterns that agree with rain gauge observations. This skill is higher over ocean than land, and it is least skillful over land with high elevation. Therefore, we will interpret our results with caution.

The ERA-Interim reanalysis dataset (Berrisford et al. 2011; Dee et al. 2011) from the European Centre for Medium-Range Weather Forecasts (ECMWF) is used in this study for TC trajectory identification and moisture transport calculations. It produces 6-hourly analyses at 0000, 0600, 1200, and 1800 UTC. Variables used in this study include temperature, winds, vorticity, and specific humidity on pressure levels and vertically integrated moisture fluxes and their divergence. Variables provided in the original truncation (truncation at wavenumber 255; T255) are used to identify TC trajectories; variables for the moisture transport calculations are gridded onto a 512 longitude $\times$ 256 latitude regular grid with a resolution of $0.7° \times 0.7°$.

### b. TC feature tracking methodology

TC trajectories used in this study are obtained from an objective feature tracking method. This method has been developed and described fully in Hodges (1994, 1995, 1999) and Bengtsson et al. (2007). The method is applied to 6-hourly ERA-Interim reanalysis data. It uses the vertically averaged vorticity at the levels 850, 700, and 600 hPa and truncated to T63 with the planetary

scales removed (total wavenumber $n \leq 5$). This was found to provide more coherent tracks including the pre-TC stages (e.g., easterly waves) and post-TC stages following extratropical transition (Serra et al. 2010; Hodges and Emerton 2015). At this stage all tropical disturbances are tracked. To identify TCs, additional information is added to the tracks in the form of vorticity at T63 resolution at multiple levels across 850–250 hPa. This allows for checking for the presence of a warm core and a coherent vertical structure. The criteria used for checking are the same as used in Bengtsson et al. (2007) and other studies (Strachan et al. 2013; Bell et al. 2013; Roberts et al. 2015).

TC tracks identified from the ERA-Interim reanalysis have been compared with observations in previous studies. The average annual TC numbers identified from the ERA-Interim reanalysis agree well with the International Best Track Archive for Climate Stewardship (IBTrACS) over the period of 1979–2002 (Strachan et al. 2013). A recent study by K. Hodges and P. Vidale (2016, personal communication) matches TC tracks identified from the ERA-Interim reanalysis to the IBTrACS data in 1979–2012: 95% of the TCs in the IBTrACS data are identified in the ERA-Interim reanalysis in the Northern Hemisphere and 93% in the Southern Hemisphere. The interannual variability of TC numbers is also well correlated between the ERA-Interim reanalysis and the IBTrACS data. Over the western Pacific region, the correlation coefficient is 0.57, which is significant at the 95% confidence level; the correlation coefficients are similar or higher over other TC basins (e.g., the North Atlantic and the south Indian Ocean) (Strachan et al. 2013). The lower correlation coefficient over the western Pacific region compared to other regions is largely due to uncertainties of identifying the weaker storms. This is partly due to the tracking method and the uncertainties in the ERA-Interim reanalysis, but there may also be contributions from uncertainties in the observations for weak storms and whether reporting agencies are consistent in the types of storms they include in the TC datasets used for IBTrACS (Hodges and Vidale 2017). The spatial distribution of TC tracks identified from the ERA-Interim reanalysis also agrees well with the IBTrACS. Strachan et al. (2013) show strong agreement between the ERA-Interim reanalysis and the IBTrACS in terms of TC track density, as well as TC genesis and lysis density.

### c. *Decomposition of mean-flow and eddy moisture fluxes related to TCs*

To investigate the contribution of TCs to moisture transport over EA, first the moisture flux is decomposed into time-mean and eddy (deviation from the mean) terms, using the 6-hourly ERA-Interim reanalysis during 1979–2012 [Eq. (1)]. In Eq. (1), $\mathbf{v}$ is horizontal wind and $q$ is the specific humidity (both are available on the 6-hourly time interval during 1979–2012); $\overline{\mathbf{v}}$ and $\overline{q}$ are monthly climatologies over 1979–2012, and $\mathbf{v}'$ and $q'$ are eddies (or deviations from the time-mean values) calculated as $\mathbf{v}' = \mathbf{v} - \overline{\mathbf{v}}$ and $q' = q - \overline{q}$ using 6-hourly ERA-Interim reanalysis. The first term on the right-hand side of Eq. (1), $\overline{\mathbf{v}}\,\overline{q}$, is the transport of mean moisture by the mean horizontal wind. We call this term the mean moisture transport or the mean-flow moisture flux afterward. The second, third, and fourth terms, $\overline{\mathbf{v}}q'$, $\mathbf{v}'\overline{q}$, and $\mathbf{v}'q'$, are the transport of eddy moisture by the mean horizontal wind, the transport of mean moisture by the eddy horizontal wind, and the transport of eddy moisture by the eddy horizontal wind, respectively. Altogether, we call these terms the eddy moisture transport or eddy moisture flux. Then, by using the TC location information obtained from the feature tracking method, a mask with a 5° geodesic radius around each TC eye at each 6-h time step is applied to the eddy terms to identify eddies that are related to the TC and mask out those that are not related [Eq. (2)]. Therefore, the eddy terms in Eq. (1) are further decomposed into TC-related terms and non-TC-related terms in Eq. (2). In the following analysis, we focus on the mean-flow moisture flux and the eddy moisture fluxes that are related to TCs. Although the size of a TC varies from storm to another, the choice of a 5° radius is an established method of differentiating TC-related features from their surroundings that has been discussed and applied by previous studies (Englehart and Douglas 2001; Larson et al. 2005; Jiang and Zipser 2010; Prat and Nelson 2013).

$$\begin{aligned}\mathbf{v}q &= (\overline{\mathbf{v}} + \mathbf{v}')(\overline{q} + q') \\ &= \overline{\mathbf{v}}\,\overline{q} + \overline{\mathbf{v}}q' + \mathbf{v}'\overline{q} + \mathbf{v}'q', \qquad (1)\end{aligned}$$

$$\begin{aligned}\mathbf{v}q &= (\overline{\mathbf{v}} + \mathbf{v}'_{\text{TC}} + \mathbf{v}'_{\text{non-TC}})(\overline{q} + q'_{\text{TC}} + q'_{\text{non-TC}}) \\ &= \overline{\mathbf{v}}\,\overline{q} + \underbrace{\overline{\mathbf{v}}q'_{\text{TC}} + \mathbf{v}'_{\text{TC}}\overline{q} + \mathbf{v}'_{\text{TC}}q'_{\text{TC}}}_{\text{TC related}} \\ &\quad + \underbrace{\overline{\mathbf{v}}q'_{\text{non-TC}} + \mathbf{v}'_{\text{non-TC}}\overline{q} + \mathbf{v}'_{\text{non-TC}}q'_{\text{non-TC}}}_{\text{non TC related}}. \qquad (2)\end{aligned}$$

Similar to the method for decomposing the moisture flux, the mask with 5° geodesic radius around each TC eye at each time step is also applied to 3-hourly TRMM 3B42 rainfall to separate TC-related rainfall from non-TC-related rainfall. Note that the temporal interval of the tracked TC position is 6 h; therefore when filtering 3-hourly TRMM 3B42 rainfall, the same mask is applied to two consecutive time steps of TRMM rainfall. We assume that the movement of a TC is small within 6 h, relative to the diameter of the masking circle.

The extreme daily rainfall on each grid is defined as the daily rainfall above the 95th percentile of rainfall in each month during 1998–2012.

## 3. Statistics of TCs over East Asia

There are 851 TCs tracked over the WNP and EA during 1979–2012. These TCs are divided into two groups according to their propagation directions: westward and northward. The westward-moving TCs are generated over the Pacific warm pool east of the Philippines and then move westward/northwestward in a straight line and make landfall along the coasts of south China or the Indochina Peninsula. The northward-moving TCs are also generated over the Pacific warm pool, but instead of hitting the coast and moving farther west, these TCs curve toward the north and make landfall over eastern China, the Korean Peninsula, or Japan. This division is similar to that in Camargo et al. (2007a), who used cluster analysis to divide TC trajectories over the WNP and EA into seven clusters that can be further grouped as straight-movers and recurvers. In general, westward-moving TCs are similar to the straight-movers in Camargo et al. (2007a), and northward-moving TCs are similar to the recurvers. Camargo et al. (2007a) found that the seven clusters in their analysis show different characteristics in terms of genesis position and lifetime. However, when comparing the difference in landfall locations, the seven clusters merged into two groups according to their trajectories (straight-mover or recurver). As we focus on the contribution of TCs to precipitation and moisture fluxes over the EA landmass, this remerging of the seven clusters into two groups based on landfall location gives us confidence to use the much simpler straight-mover/recurver (westward/northward) classification to carry out our study.

The number of TCs in each month and in each group over the period of 1979–2012 is shown in Fig. 1. There are more northward-moving TCs than westward-moving TCs in each month, which is consistent with results shown in other datasets (e.g., IBTrACS) (Camargo et al. 2007a). TC activity over the WNP and EA shows a single peak in the mean seasonal cycle. More in detail, westward-moving TCs are rare from January to May, then increase from July to October (JASO) with the highest number in October; northward-moving TCs show a similar seasonal cycle, being inactive from December to April and active during JASO, with the highest number occurring in September. 58% of all TCs over the WNP and EA occur during JASO. After peaking, TC activity over the WNP and EA decreases rapidly.

These seasonal features over the WNP and EA are similar to those for global TCs, which are due to a number of factors, such as the mean seasonal cycle SST, which is positively correlated with mean seasonal cycle of TC frequency, a low vertical wind shear in the atmosphere, and the existence of a monsoon trough or easterly waves. However, other features, such as the division of westward and northward trajectories, are unique and relate to the positions of the EA summer monsoon trough and the WNPSH. We find similar statistics to 1979–2012 for the 1998–2012 period of the TRMM rainfall record (not shown). During season JASO, there are 14.6 TCs per season over the period 1979–2012 and 14.0 TCs per season over the period 1998–2012.

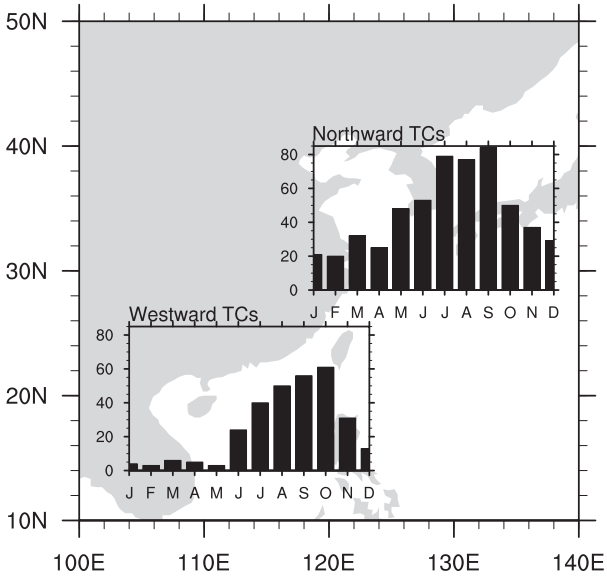


FIG. 1. Monthly counts of westward- and northward-moving TCs over EA (10°–50°N, 100°–140°E) during 1979–2012. TCs are identified from the ERA-Interim reanalysis using the TC feature tracking method.

## 4. Fractional contribution to rainfall

The monthly mean fractional contribution of TC rainfall to total rainfall during 1998–2012 is shown in Fig. 2. TC rainfall makes larger fractional contributions during JASO over both the WNP and the coast of EA. In other months, the TC contribution is small and confined to the WNP warm pool. Only the Indochina Peninsula is affected by TCs in November–January. Note that there are some spotted contributions over the midlatitudes in December–February. This is caused by midlatitude disturbances that have been identified as TCs and thus been included in the analysis here. However, the contributions from these midlatitude disturbances are negligible.

During JASO, the average contribution of TC rainfall over the southeastern coast of China is 10%–30%. The contribution is larger at lower latitudes, especially over islands (e.g., Taiwan, Hainan Island, and the Philippines),

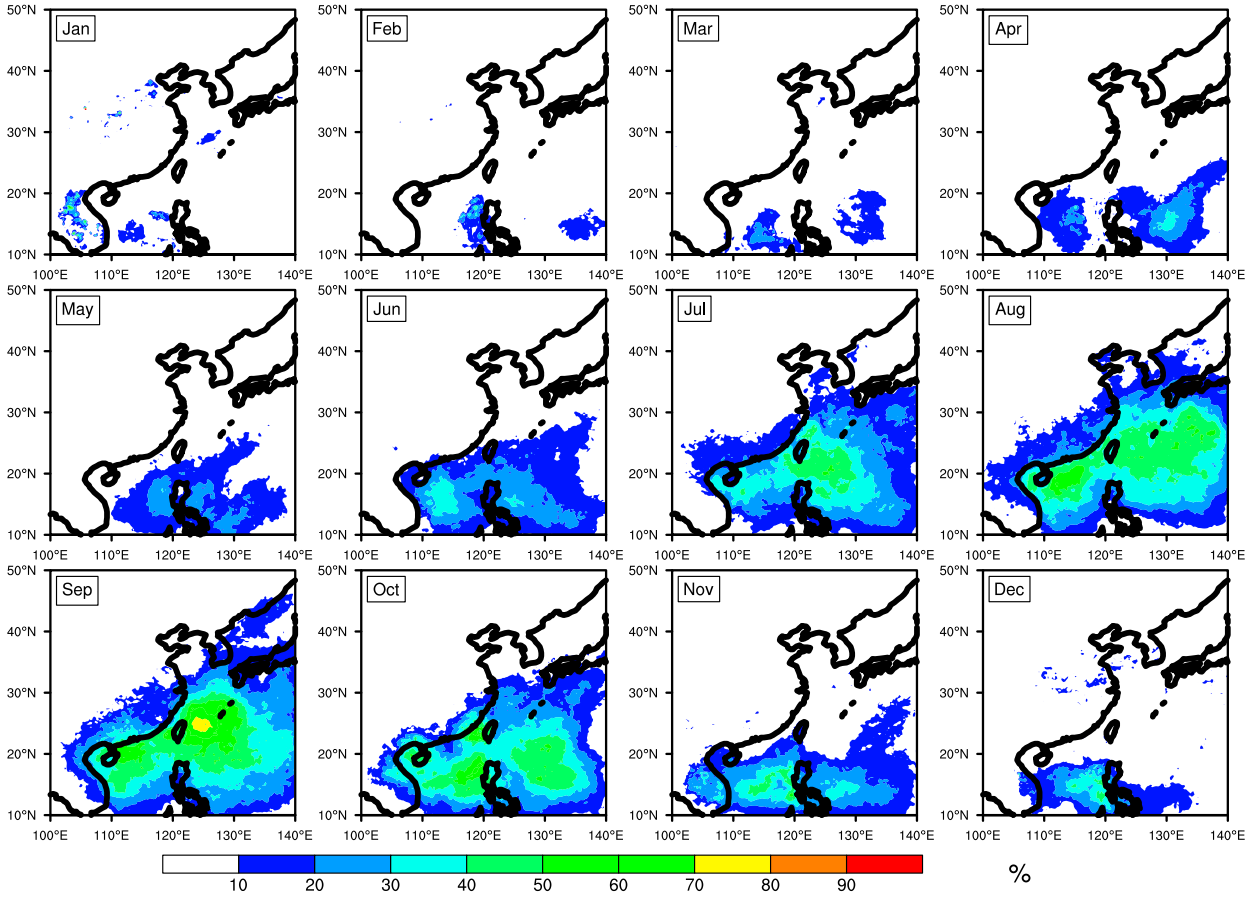


FIG. 2. Contribution of TCs to monthly rainfall, calculated using TRMM 3B42 rainfall data for 1998–2012. Units: %.

where the contribution is as high as 40%–50%. At higher latitudes (e.g., the Bohai Bay, the Korean Peninsula, and southern Japan), TCs make a substantial contribution to total rainfall only in August and September. The spatial pattern of the contribution of TC rainfall matches closely with the TC number shown in Fig. 1. With most northward-moving TCs occurring in September, the impact of TCs reaches as far north as 45°N in that month; since most westward-moving TCs occur in October, the TC rainfall contribution also reaches its maximum over the Indochina peninsula in October.

Heavy rainfall caused by TCs after landfall can cause flooding and other losses. Therefore, it is necessary to quantify the TC contribution to extreme rainfall over EA. We define an extreme rainfall day as the occurrence of daily rainfall above a threshold of the 95th percentile; the threshold is computed for each month and grid point using data for 1998–2012. We compute the contribution of TCs to both the occurrence and amount of extreme rainfall during JASO. (In other months, these contributions are negligible over EA.) For occurrence, at each grid point we compute the percentage of extreme rainfall days on which a TC is within the area defined by a circle with a 5° geodesic radius around that grid point. If there were no relationship between TCs and extreme rainfall occurrence, this percentage would be 5%. For amount, at each grid point we compute the percentage of the total amount of extreme rainfall (summed over all extreme days) that occurs on TC days. The contribution of TCs to extreme rainfall occurrence is shown in the upper panels of Fig. 3. In general, the contribution of TCs to extreme rainfall occurrence is higher than to total rainfall, which indicates that rainfall intensity during TCs is above average. Over the ocean, the contribution to occurrence is over 70%, which means that on over 70% of days on which daily rainfall exceeds the 95th percentile there is a TC within a 5° radius of the grid point; this contribution is over 90% in September and October, especially to the east of Taiwan and the Philippines. Over Taiwan, TCs appear on more than 70% of extreme rainfall days; this contribution can also reach 60% over Hainan Island and the northern Philippines. Along the southern China coast and the Indochina Peninsula, this contribution is also over 50%, which is higher than the TCs contribution to total rainfall.

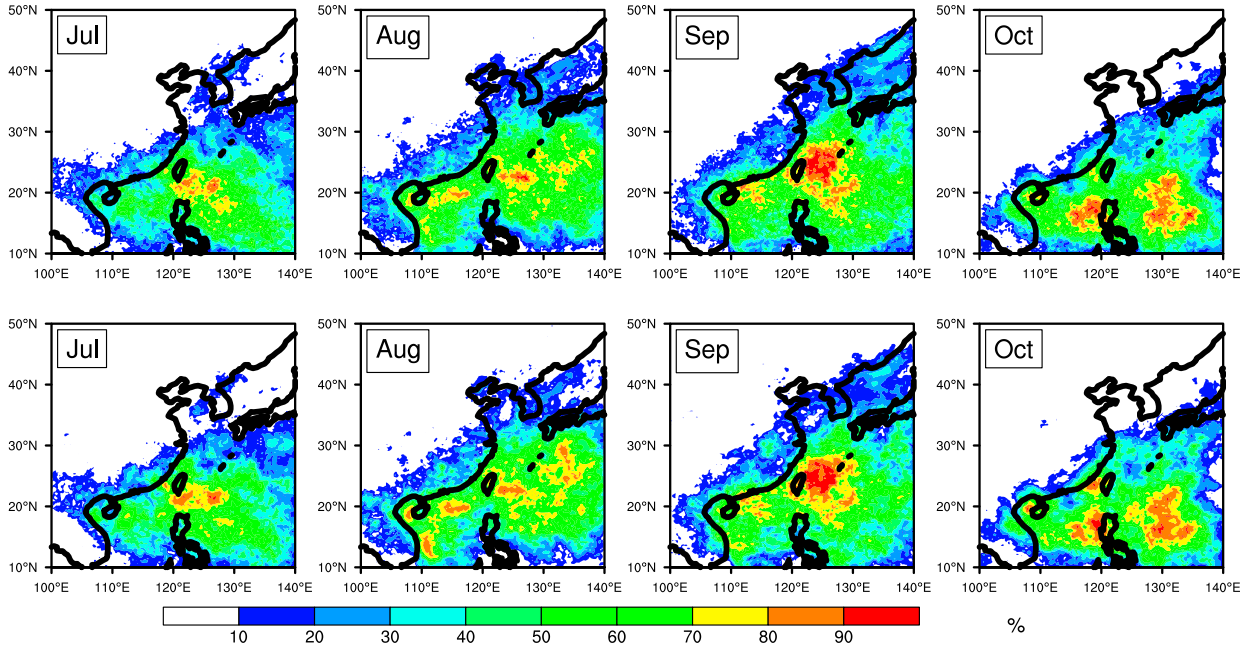


FIG. 3. Monthly contributions of TCs to (top) extreme rainfall occurrence and (bottom) extreme rainfall amounts, calculated using TRMM 3B42 rainfall data for 1998–2012. Units: %.

The contribution of TCs to extreme rainfall amount is shown in the lower panel of Fig. 3. Comparing the TC contributions to occurrence and amount allows us to measure whether extreme rainfall related to TCs is heavier than extreme rainfall that is unrelated to TCs. If this were the case, then the TC contribution to extreme rainfall amount would be higher than the contribution to extreme rainfall occurrence. As shown in Fig. 3, the spatial distribution of contributions to extreme rainfall amount is similar to the contributions to extreme rainfall occurrence (the pattern correlation between maps of these diagnostics for each month varies between 0.8 and 0.99). However, there are regions where the contributions to extreme rainfall amount are higher than the contributions to extreme rainfall occurrence. For example, over the Anhui Province of China (30°N, 117°E) in September, the contributions to extreme rainfall occurrence are about 30%–40%, while the contributions to extreme rainfall amount are about 50%. This difference indicates that TC-related extreme rainfall over these regions is heavier than extreme rainfall that is unrelated to TCs.

## 5. Moisture flux: Relative contributions of eddy (TC) transport and mean flow

As EA is affected by one of the most prominent monsoon systems, the warm and moist monsoonal flow brings a large amount of moisture over land. Generated over the warm and moist ocean, TCs also gather and transport moisture along their paths. With TC landfalls, moisture convergence associated with TCs is therefore a contributor to the water budget over EA.

To compare the roles of TCs and the EASM in the process of moisture transport, Fig. 4 shows monthly accumulated moisture flux divergence due to both the mean, $\nabla \cdot (\overline{\mathbf{v}}\,\overline{q})$, and the TC eddy moisture transport, $\nabla \cdot (\overline{\mathbf{v}}q'_{\mathrm{TC}} + \mathbf{v}'_{\mathrm{TC}}\overline{q} + \mathbf{v}'_{\mathrm{TC}}q'_{\mathrm{TC}})$. The mean-flow moisture flux divergence shows features arising from the EASM (the upper panel of Fig. 4), that is, a moisture convergence band that represents the mei-yu front (shown in Fig. 4 by the ridge of the WNPSH at 500 hPa) stretches from central China to Japan in July and August and then shifts southward to the southern China in September; the band then withdraws farther south to the Indochina Peninsula in October and eventually fades away from the most of the EA landmass.

The TC eddy moisture flux divergence is smaller in amplitude and also in spatial extent compared to the mean-flow moisture flux divergence (the lower panel of Fig. 4). However, TC moisture flux divergence shows a different seasonal cycle from the mean EASM moisture flux divergence (i.e., the mean-flow moisture flux convergence prevails over the EA during JJA, whereas the TC moisture flux convergence affects EA during JASO). The spatial patterns of moisture flux convergence are also different between the EASM and TCs.

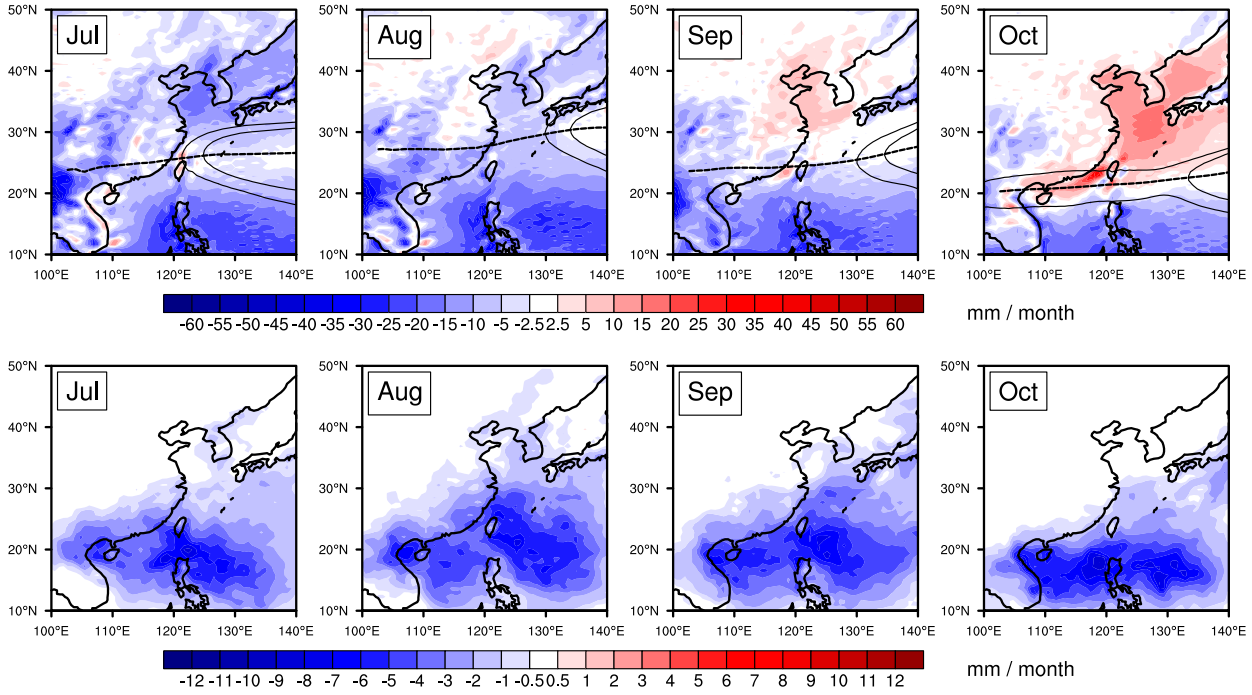


FIG. 4. Monthly accumulated vertically integrated moisture flux divergence for the (top) mean moisture transport $[\nabla \cdot (\bar{\mathbf{v}}\bar{q})]$ and (bottom) TC eddy moisture transport $[\nabla \cdot (\bar{\mathbf{v}}q'_{\mathrm{TC}} + \mathbf{v}'_{\mathrm{TC}}\bar{q} + \mathbf{v}'_{\mathrm{TC}}q'_{\mathrm{TC}})]$ (averaged over 1979–2012). Units: mm month$^{-1}$. The dashed line in the upper panel indicates the ridge of NWPSH at 500 hPa; Solid lines are geopotential height at 5875 and 5880 m.

The position of the mei-yu front, where the mean-flow moisture flux convergence dominates, depends on the positions of the monsoon trough and the ridge of the WNPSH, while the pattern of TC moisture flux convergence depends on the number and trajectories of TCs.

Therefore, the TC moisture flux convergence is not negligible with respect to the mean-flow moisture flux convergence; their contributions to the water cycle come in different regions and at different times. In July, when the mei-yu front is located at around 30°N, the mean-flow moisture flux comes from the south and converges along the mei-yu front. Meanwhile, southern China loses moisture due to mean-flow moisture flux divergence. However, for TCs, there are more westward-moving TCs moving into southern China in July, which import moisture that is required to maintain rainfall over this region. In August, when the intensity of the NWPSH weakens and the mei-yu front deflects to the south, the mean-flow moisture flux convergence becomes the main moisture supplier over southern China again. For TCs, there are more northward-moving TCs in August, which bring moisture to higher latitudes including Baohai Bay, the Korean Peninsula, and Japan; the TC moisture flux replaces the mean-flow moisture flux as the main supplier of moisture over northern China. TCs reach their peak in September, when the mean-flow moisture flux weakens and the mei-yu front withdraws farther south to the south coast of China and the Indochina Peninsula, and play a more important role in transporting moisture to the north. In October, when the EASM has completely faded away from EA, TCs remain as the main moisture supplier to EA, especially along the coast. TCs are able to transport moisture beyond the coastal regions to further inland, but their reach does not extend as far inland as that of the mean flow.

The seasonal cycle of monthly mean vertically integrated moisture flux passing through the coastal boundaries of EA is shown in Fig. 5. Two boundaries are defined, shown in the inner panel of Fig. 5: an eastern (meridional) boundary at 121°E between 21° and 43°N, and a southern (zonal) boundary at 21°N between 100° and 121°E. Because there is little moisture transported from the north, we do not use a northern boundary. Although there is significant mean moisture transported from the west during the Indian monsoon season, the TC moisture transported from the west remains small as most TCs move westward or northward over EA. Therefore, moisture transported into the EA region from the west is not included in this comparison of the mean flow and TCs.

The seasonal cycles of the mean-flow moisture fluxes on both boundaries show a clear EASM cycle. At the southern boundary, moisture is transported into EA between February and August. This period can be

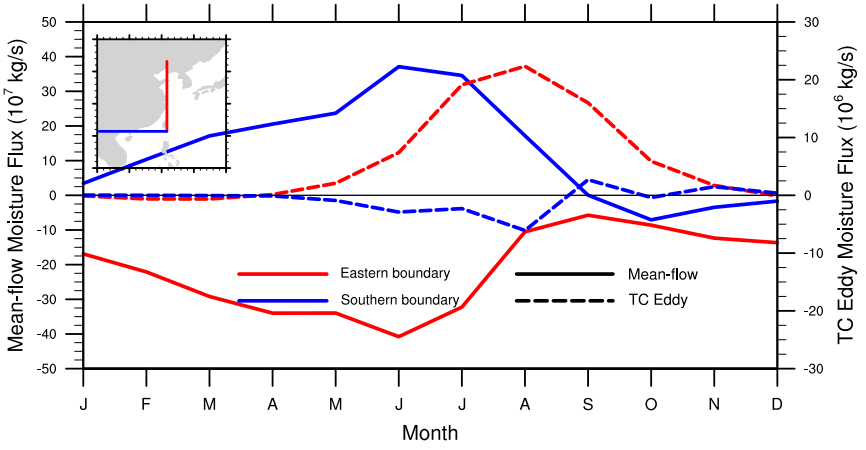


FIG. 5. Seasonal cycle of monthly mean vertically integrated moisture flux passing through the southern (blue) and eastern (red) boundaries. The mean-flow moisture fluxes are shown as solid lines (using the left-hand vertical axis) and TC eddy moisture fluxes as dashed lines (using the right-hand vertical axis). The inner panel shows the definition of the southern and eastern boundaries. Positive (negative) values indicate moisture is transported into (out of) the EA landmass. Note that the scale of the right-hand vertical axis is an order of magnitude smaller than the left-hand vertical axis. Unit: kg $s^{-1}$.

further divided into two subphases. From late February to early May, the mean-flow moisture influx is small and supplies moisture for the spring rainfall (Tian and Yasunari 1998) over southeastern China; from late May to August, the mean-flow moisture influx increases and supplies moisture for the EASM. This moisture is brought in by both the westerly flow from the Indian Ocean, extending from the Indian monsoon circulation, and the western flank of the WNPSH, which are the dominant features defining the EASM. From September to December, the winter monsoon brings dry and cold air from the north, and the mean-flow moisture flux at the southern boundary is negative. At the eastern boundary, the mean-flow moisture flux is almost opposite to that at the southern boundary. Moisture imported to EA via the southern boundary is exported from the eastern boundary. This outflow is particularly important to several East Asian regions (i.e., the Korean Peninsula and Japan), as it is the main moisture supply during JJA.

The TC moisture fluxes on both boundaries are an order of magnitude smaller than the mean fluxes. However, the seasonal cycles of TC moisture fluxes on both boundaries are different from the mean-flow fluxes. In general, instead of showing a maximum moisture flux during JJA, TC moisture fluxes peak during JASO, consistent with the seasonal distribution of TC frequency shown in Fig. 1. Instead of gaining moisture from the southern boundary and losing moisture from the eastern boundary like the mean-flow moisture fluxes, the direction of TC moisture fluxes is opposite. That is, TC moisture flux causes a net import at the eastern boundary and a net export at the southern boundary.

To understand this difference in moisture transport between the mean flow and TCs, case studies for different types of TCs are carried out. Figure 6 shows the total TC moisture fluxes and their divergence for two different TCs: a westward-moving TC (Tai-Kat) and a northward-moving TC (Masta). In a single time step, the TC moisture flux shows a cyclonic circulation with predominant convergence (not shown). As the TC moisture flux is summed along its trajectory (multiple time steps) for either a westward-moving or a northward-moving TC, the cumulative TC moisture flux is modified due to the partial overlap of the 5° circles around the TC on consecutive time steps; that is, the front of a TC in its direction of travel at the $n$th time step is overlapped by the rear part of a TC at the $(n + 1)$th time step. Because of the cyclonic flow around the TC, the direction of the wind (and hence the moisture transport) reverses, such that the cumulative TC moisture flux is weakened in the TC area along the trajectory. Meanwhile, TC moisture fluxes at the edges of the TC area orthogonal to the direction of propagation remain strong or even are strengthened, because the moisture flux retains its sign as the TC propagates. As shown in Fig. 6, there are strong forward fluxes (same direction as the TC propagation direction) to the right of a TC, and strong rearward flux (opposite direction to the TC propagation direction) to the left of a TC. This is the case for either westward-moving TCs or northward-moving TCs. As most westward-moving TCs

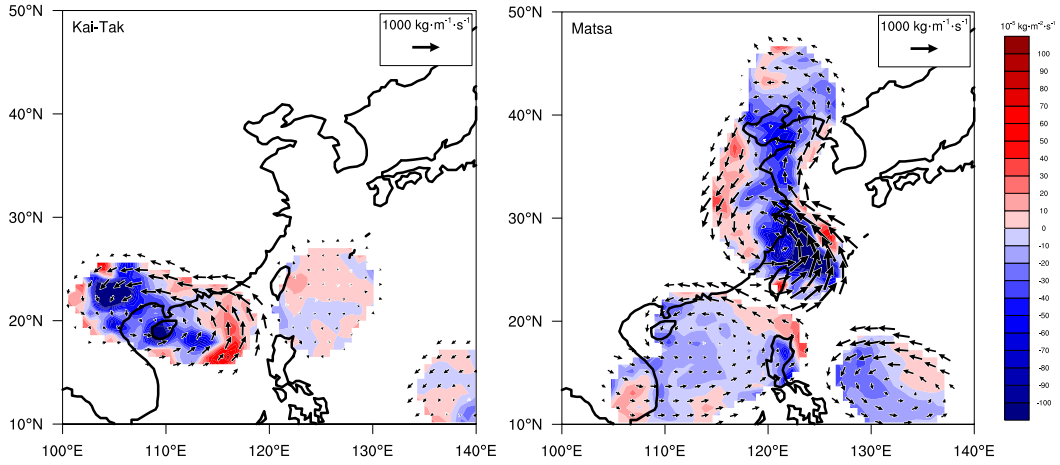


FIG. 6. Moisture flux (vector) and its divergence (shading) during (a) the westward-moving TC Tai-Kat (11–18 Aug 2012) and (b) the northward-moving TC Matsa (1–12 Aug 2005). In the text, we only discuss the features with strongest magnitude, which belong the TCs named above. The weaker signals northeast of the Philippines in (a) and east and west of the Philippines in (b) belong to other, weaker TCs that are not discussed in the text.

appear to the south of the EA landmass (between 15° and 25°N, as shown in Fig. 8), the south/southeast coast of China is exposed to the easterly moisture flux prevailing to the right of these TCs. Therefore, TC moisture fluxes enter the EA region from the eastern boundary during the active period (JASO).

A similar argument applies to the northward-moving TCs and moisture export from the southern boundary. With northward-moving TCs approaching the coast of EA, the northerly moisture flux to the left of the direction of propagation of these TCs has a large impact. Therefore, there is an export of moisture at the southern boundary during the TC active period. Note that the moisture export at the southern boundary is smaller than the moisture import at the eastern boundary. This could be because the propagation direction of TCs and the direction of moisture flux are opposite to each other at the southern boundary, which reduces the intensity of moisture flux. This could also be because the moisture flux at the southern boundary is weaker than the moisture flux at the eastern boundary due to drier air. The easterly moisture flux at the eastern boundary is imported directly from the warm and humid ocean, but the northerly moisture flux at the southern boundary is exported from the EA landmass. After weakening and drying as a result of the rough land surface and the lack of moisture supply from the ocean, the TC intensity is reduced. For all these reasons, only a fraction of moisture is exported at the southern boundary compared to the moisture imported at the eastern boundary.

We also note that the export of moisture at the southern boundary disappears after August and changes sign in September. This is due to changes in the background meridional specific humidity gradient (Fig. 7). The mean specific humidity field shows a reversed meridional gradient during JJA (i.e., higher humidity in the subtropics than at the equator) and a normal meridional gradient before and after JJA. The reversed specific humidity gradient is due to the strong mean moisture flux convergence and high land surface temperature over EA during the EASM. As shown in Eq. (2), the TC eddy moisture flux is composed of three terms ($\overline{\mathbf{v}}q' + \mathbf{v}'\overline{q} + \mathbf{v}'q'$). Among them, the second term (i.e., the mean specific humidity transported by TC eddies) dominates (not shown). Therefore, when comparing the TC moisture flux in August and September, although the TC eddies themselves are similar in structure, the TC moisture flux changes its sign due to the reversed moisture meridional gradient.

Another interesting point is that, as shown in Fig. 8, although September and October feature more westward-moving TCs (57 and 62 TCs, respectively), the TC moisture flux transport through the eastern boundary is smaller compared to that of August or July, which have 40 or 52 westward-moving TCs, respectively. This is due to the seasonal shift of TC locations: any TC that contributes to moisture flux on the eastern boundary needs to be located north of 16°N between 100° and 121°E (the dotted line in Fig. 8). In September, 54% of the westward-moving TCs appear to the north of this line, and this proportion decreases to 24% in October. Although there are fewer total westward-moving TCs in July and August, there are more westward-moving TCs north of 16°N (90% in July and 73% in August). The range and position of WNPSH shown in Fig. 4 also indicate changes in background circulation that contribute to this shift. In October, the WNPSH locates at lower

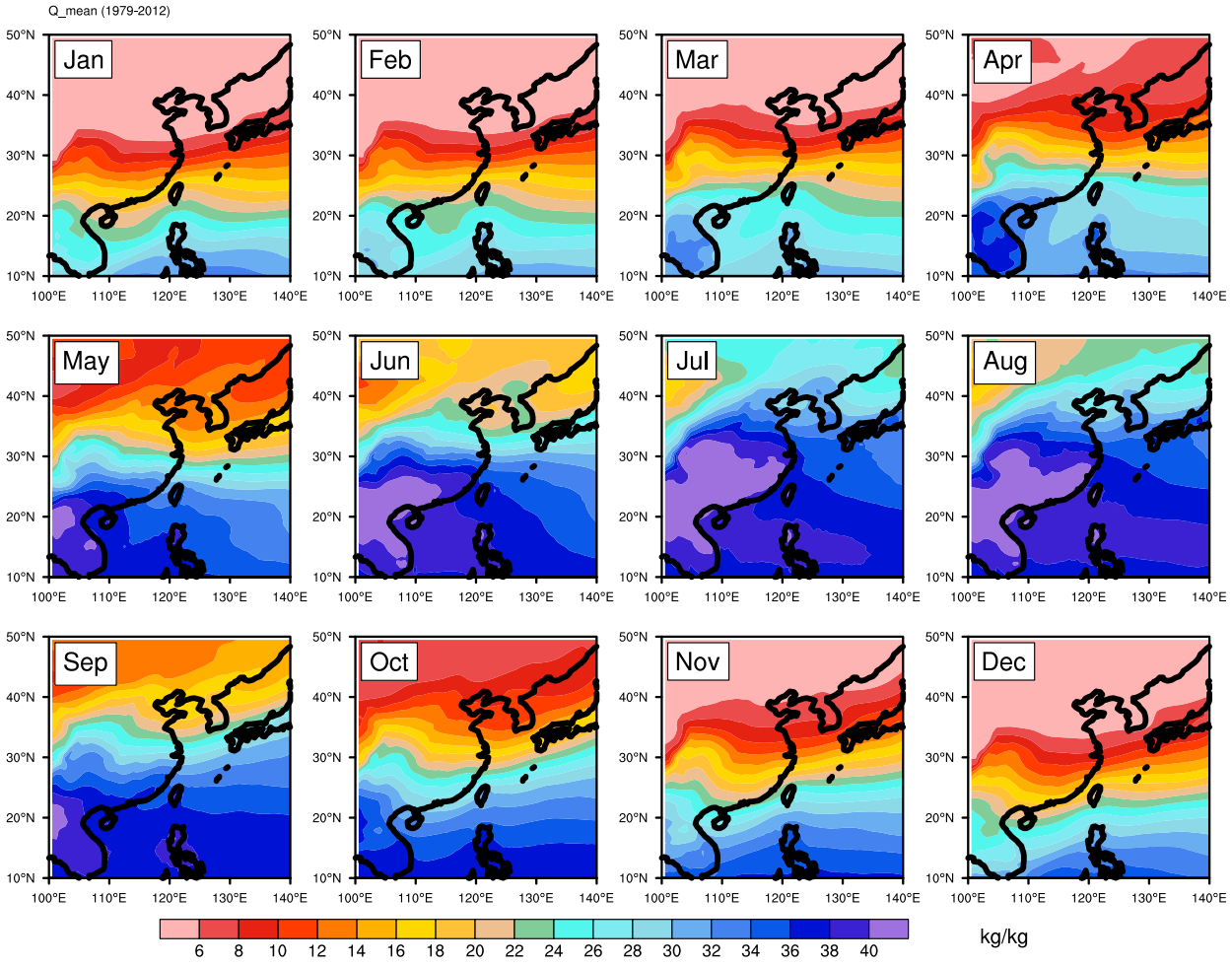


FIG. 7. Monthly mean vertically integrated specific humidity during 1979–2012. Unit: kg kg$^{-1}$.

latitude and is elongated from the east of Philippine westward to reach the Indo-China Peninsula. The easterlies along the southern flank of the WNPSH favor more westward-moving TCs and, because of its low latitude, more TCs are located to the south of 16°N.

## 6. Conclusions and discussion

This study was motivated by the need to quantify the contributions of TCs to the water budget over EA, especially over China. Previous studies in this field have focused either on the drivers of TC variability on temporal scales from intraseasonal to decadal, or on the contribution of TCs to rainfall. This study is therefore an attempt to bridge the gap between studies that investigate TC variations and studies that focus only on the TC contribution to rainfall over EA. This study retains its focus on the climatological contributions of TCs' atmospheric moisture transport, as well as extreme and total rainfall. We found a distinct seasonal cycle and direction of moisture transport by TCs when compared to the mean moisture transport associated with the EASM.

In this study, TC tracks over the WNP and EA were first identified by applying an objective feature tracking method to the ERA-Interim 6-hourly reanalysis (1979–2012). Compared with the observation dataset IBTrACS, the correspondence between these two sets of data is 95%–98% over the western North Pacific and East Asia (Strachan et al. 2013; Roberts et al. 2015). According to TC tracks, TCs over the WNP and EA are separated into two groups according to propagation direction: the westward and northward-moving TCs. The TC seasonal frequency histograms from 1979 to 2012 show that JASO is the active season for both groups of TCs, accounting for 58% of the overall number over the WNP and EA.

Consistent with the seasonal cycle in TC numbers, during JASO, TC rainfall has the largest contribution over the EA coast, with an averaged contribution between 10% and 30% of the total rainfall. TC rainfall

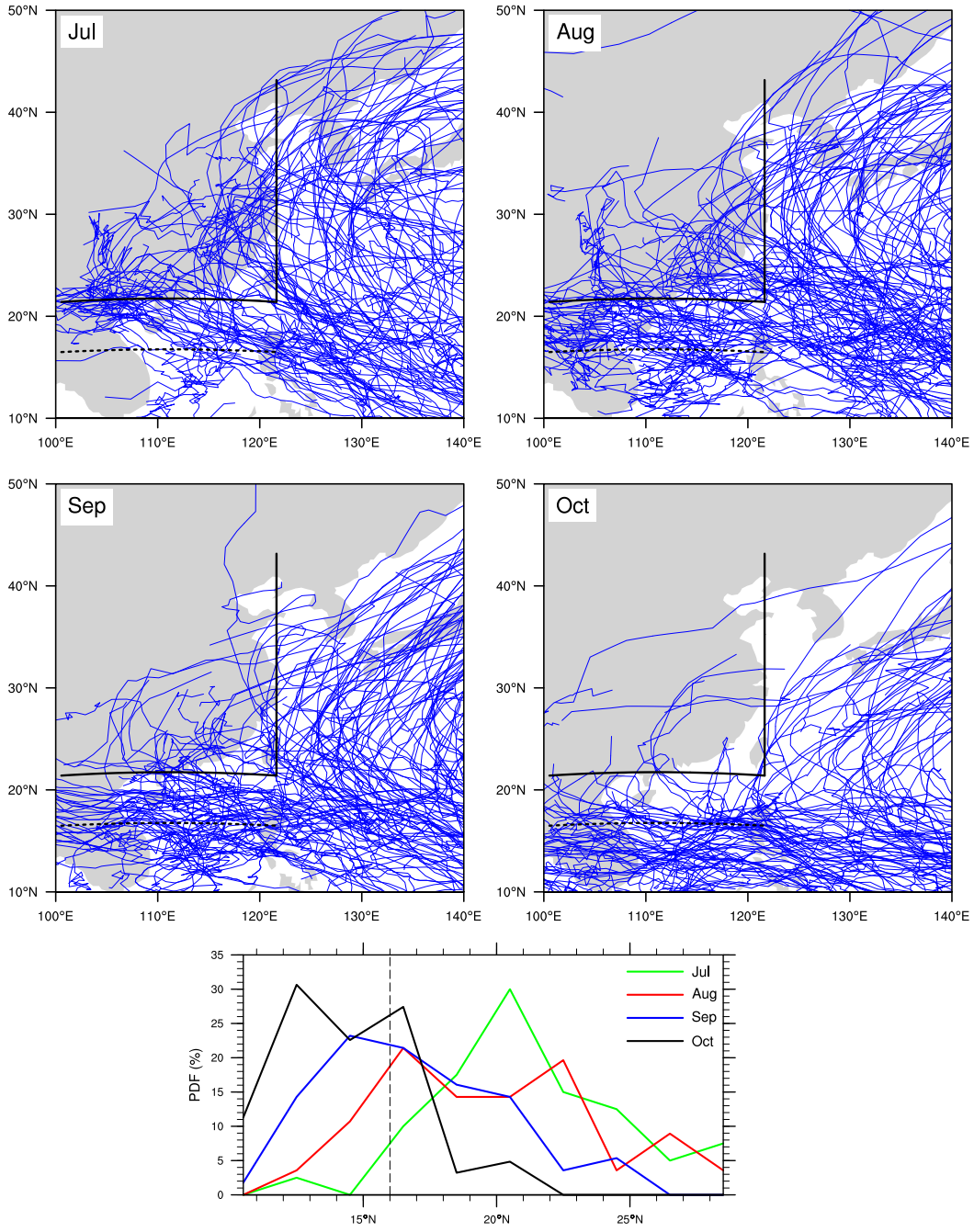


FIG. 8. (top four panels) Identified TC tracks in each month of JASO during 1979–2012 using the ERA-Interim reanalysis. The two solid black lines show the eastern (21°–42°N, 121°E) and southern (21°N, 100°–121°E) boundaries from Fig. 5; the dotted line is at 16°N, 100°–121°E). (bottom) The PDF of westward-moving TCs distributing along latitude for each month (Jul–Oct) averaged between 100° and 121°E. A reference line is drawn at 16°N.

reaches as far north as 45°N in September for the northward-moving TCs and has its maximum impact over the Indochina Peninsula for the westward-moving TCs in October. TC rainfall contribution is largest over the tropical islands (i.e., Taiwan, the Philippines, and Hainan Island), with contributions as high as 50% of the total rainfall.

TC rainfall contributions to the extreme daily rainfall (above the 95th percentile) are investigated in terms of occurrence and amount. The contribution of TCs to the

occurrence of extreme daily rainfall is around 50% over the EA coast. This contribution is higher (60%–70%) over tropical islands. The TC contribution to the extreme rainfall amount is higher in percentage than the contribution to the extreme rainfall occurrence over some regions (e.g., the Anhui Province of China along the Yangtze River Valley). This indicates that TC-related extreme rainfall over these regions is heavier than extreme rainfall unrelated to TCs.

Because of different seasonal cycles, moisture transport associated with TCs is another important source for the EA water budget, although its magnitude is smaller than the mean-flow moisture transport associated with the climatological EASM. The mean-flow moisture transport reaches a maximum during JJA and features a moisture convergence band (the mei-yu front) marching north in July and gradually withdrawing to the south in the following months. The TC moisture transport reaches a maximum during JASO; it is an important moisture supplier especially after the EASM withdraws.

The pathways of moisture flux transported by the mean flow and TCs also show different patterns. For the mean flow, moisture is imported from the south and exported to the east with its maximum during the EASM season (JJA). For TCs, moisture is imported from the east and exported to the south during the TC active season (JASO). This different pattern of TC moisture transport is closely related to TC propagation directions, changes in the mean meridional humidity gradient, and the shift of TC positions with large-scale background flow during the season.

The diagnostics conducted in the study have been repeated with the IBTrACS data and show similar results. Quantitative differences, however, are found. The TC moisture fluxes via both boundaries (as defined in Fig. 5) are larger by using the IBTrACS data. It is about 20% larger for the TC moisture influx via the eastern boundary during the TC peak season. The difference in the net TC moisture flux is less than 10% due to the larger TC moisture efflux via the southern boundary during the TC peak season. Also, the sign change of TC moisture flux in September on the southern boundary is delayed to October while using the IBTrACS tracks. Nevertheless, results from both TC tracks support the same conclusions.

A major aim of this study was to identify and quantify the contribution of TCs to rainfall and the water budget over EA, especially China. However, simulating rainfall over EA remains a challenge for state-of-the-art general circulation models (GCMs) (Sperber et al. 2013; Song and Zhou 2014). As TCs make an important contribution to the rainfall and water budget over EA, it is essential that models represent accurately not only the characteristics of TCs themselves, but also their impacts on the large-scale atmospheric environment. The TC feature tracking method used in this study offers an opportunity to compare TC activity in model simulations to reanalysis data using an identical method. It will be valuable to assess model simulations using the analysis techniques developed this study, especially for sensitivity tests with a single model (e.g., tests of horizontal resolution or of atmosphere–ocean feedbacks). Roberts et al. (2015) (and references therein) showed that model resolution is crucial for a realistic simulation of TC behavior and variability, and higher-resolution GCMs are increasingly able to capture TC intensity and the large-scale environmental conditions that contribute to tropical cyclogenesis. To further understand the water budget over this region, contributions from other components need to be quantified. This will also help to identify deficits in model simulations and improve the skill of climate prediction and weather forecasting over this region.

*Acknowledgments.* The authors thank Kevin Hodges for discussions and comments, especially on the feature checking methodology; the authors appreciate discussions with Malcolm Roberts. This work and its contributors were supported by the UK-China Research and Innovation Partnership Fund through the Met Office Climate Science for Service Partnership (CSSP) China as part of the Newton Fund. NPK was also funded by a UK Natural Environment Research Council Independent Research Fellowship (NE/L010976/1).

## REFERENCES

Bell, R., J. Strachan, P. L. Vidale, K. Hodges, and M. Roberts, 2013: Response of tropical cyclones to idealized climate change experiments in a global high-resolution coupled general circulation model. *J. Climate*, **26**, 7966–7980, doi:10.1175/JCLI-D-12-00749.1.

Bengtsson, L., K. I. Hodges, and M. Esch, 2007: Tropical cyclones in a T159 resolution global climate model: Comparison with observations and re-analysis. *Tellus*, **59A**, 396–416, doi:10.1111/j.1600-0870.2007.00236.x.

Berrisford, P., and Coauthors, 2011: ERA-Interim archive, v2. ECMWF Tech. Rep. 23, 96 pp.

Camargo, S. J., A. W. Robertson, S. J. Gaffney, P. Smyth, and M. Ghil, 2007a: Cluster analysis of typhoon tracks. Part I: General properties. *J. Climate*, **20**, 3635–3653, doi:10.1175/JCLI4188.1.

——, ——, ——, ——, and ——, 2007b: Cluster analysis of typhoon tracks. Part II: Large-scale circulation and ENSO. *J. Climate*, **20**, 3654–3676, doi:10.1175/JCLI4203.1.

Chan, J. C. L., 2000: Tropical cyclone activity over the western North Pacific associated with El Niño and La Niña events. *J. Climate*, **13**, 2960–2972, doi:10.1175/1520-0442(2000)013<2960:TCAOTW>2.0.CO;2.

Chen, J., R. Wu, and Z. Wen, 2012: Contribution of South China Sea tropical cyclones to an increase in southern China summer rainfall around 1993. *Adv. Atmos. Sci.*, **29**, 585–598, doi:10.1007/s00376-011-1181-6.

Chen, J.-M., T. Li, and C.-F. Shih, 2010: Tropical cyclone– and monsoon-induced rainfall variability in Taiwan. *J. Climate*, **23**, 4107–4120, doi:10.1175/2010JCLI3355.1.

Chen, Y., E. E. Ebert, K. J. Walsh, and N. E. Davidson, 2013: Evaluation of TRMM 3B42 precipitation estimates of tropical cyclone rainfall using PACRAIN data. *J. Geophys. Res.*, **118**, 2184–2196, doi:10.1002/jgrd.50250.

Chia, H., and C. Ropelewski, 2002: The interannual variability in the genesis location of tropical cyclones in the northwest Pacific. *J. Climate*, **15**, 2934–2944, doi:10.1175/1520-0442(2002)015<2934:TIVITG>2.0.CO;2.

Dare, R. A., N. E. Davidson, and J. L. McBride, 2012: Tropical cyclone contribution to rainfall over Australia. *Mon. Wea. Rev.*, **140**, 3606–3619, doi:10.1175/MWR-D-11-00340.1.

Dee, D. P., and Coauthors, 2011: The ERA-Interim reanalysis: Configuration and performance of the data assimilation system. *Quart. J. Roy. Meteor. Soc.*, **137**, 553–597, doi:10.1002/qj.828.

Englehart, P. J., and A. V. Douglas, 2001: The role of eastern North Pacific tropical storms in the rainfall climatology of western Mexico. *Int. J. Climatol.*, **21**, 1357–1370, doi:10.1002/joc.637.

Feng, X., R. Wu, J. Chen, and Z. Wen, 2013: Factors for interannual variations of September–October rainfall in Hainan, China. *J. Climate*, **26**, 8962–8978, doi:10.1175/JCLI-D-12-00728.1.

Ho, C.-H., H.-S. Kim, J.-H. Jeong, and S.-W. Son, 2009: Influence of stratospheric quasi-biennial oscillation on tropical cyclone tracks in the western North Pacific. *Geophys. Res. Lett.*, **36**, L06702, doi:10.1029/2009GL037163.

Hodges, K. I., 1994: A general method for tracking analysis and its application to meteorological data. *Mon. Wea. Rev.*, **122**, 2573–2586, doi:10.1175/1520-0493(1994)122<2573:AGMFTA>2.0.CO;2.

——, 1995: Feature tracking on the unit sphere. *Mon. Wea. Rev.*, **123**, 3458–3465, doi:10.1175/1520-0493(1995)123<3458:FTOTUS>2.0.CO;2.

——, 1999: Adaptive constraints for feature tracking. *Mon. Wea. Rev.*, **127**, 1362–1373, doi:10.1175/1520-0493(1999)127<1362:ACFFT>2.0.CO;2.

——, and R. Emerton, 2015: The prediction of Northern Hemisphere tropical cyclone extended life cycles by the ECMWF ensemble and deterministic prediction systems. Part I: Tropical cyclone stage. *Mon. Wea. Rev.*, **143**, 5091–5114, doi:10.1175/MWR-D-13-00385.1.

——, and P. L. Vidale, 2017: How well are tropical cyclones represented in reanalysis datasets? *J. Climate*, doi:10.1175/JCLI-D-16-0557.1, in press.

Huffman, G. J., and D. T. Bolvin, 2012: TRMM and other data precipitation data set documentation. NASA GSFC, 42 pp. [Available online at ftp://precip.gsfc.nasa.gov/pub/trmmdocs/3B42_3B43_doc.pdf.]

Jiang, H., and E. J. Zipser, 2010: Contribution of tropical cyclones to the global precipitation from eight seasons of TRMM data: Regional, seasonal, and interannual variations. *J. Climate*, **23**, 1526–1543, doi:10.1175/2009JCLI3303.1.

Kim, J.-H., C.-H. Ho, H.-S. Kim, C.-H. Sui, and S. K. Park, 2008: Systematic variation of summertime tropical cyclone activity in the western North Pacific in relation to the Madden–Julian oscillation. *J. Climate*, **21**, 1171–1191, doi:10.1175/2007JCLI1493.1.

Larson, J., Y. Zhou, and R. W. Higgins, 2005: Characteristics of landfalling tropical cyclones in the United States and Mexico: Climatology and interannual variability. *J. Climate*, **18**, 1247–1262, doi:10.1175/JCLI3317.1.

Lee, M.-H., C.-H. Ho, J.-H. Kim, and H.-J. Song, 2012: Low-frequency variability of tropical cyclone-induced heavy rainfall over East Asia associated with tropical and North Pacific sea surface temperatures. *J. Geophys. Res.*, **117**, D12101, doi:10.1029/2012JD017565.

Prat, O. P., and B. R. Nelson, 2013: Mapping the world's tropical cyclone rainfall contribution over land using the TRMM Multi-satellite Precipitation Analysis. *Water Resour. Res.*, **49**, 7236–7254, doi:10.1002/wrcr.20527.

——, and ——, 2016: On the link between tropical cyclones and daily rainfall extremes derived from global satellite observations. *J. Climate*, **29**, 6127–6135, doi:10.1175/JCLI-D-16-0289.1.

Ren, F., B. Gleason, and D. Easterling, 2002: Typhoon impacts on China's precipitation during 1957–1996. *Adv. Atmos. Sci.*, **19**, 943–952, doi:10.1007/s00376-002-0057-1.

——, G. Wu, W. Dong, X. Wang, Y. Wang, W. Ai, and W. Li, 2006: Changes in tropical cyclone precipitation over China. *Geophys. Res. Lett.*, **33**, L20702, doi:10.1029/2006GL027951.

Roberts, M. J., and Coauthors, 2015: Tropical cyclones in the UPSCALE ensemble of high-resolution global climate models. *J. Climate*, **28**, 574–596, doi:10.1175/JCLI-D-14-00131.1.

Serra, Y. L., G. N. Kiladis, and K. I. Hodges, 2010: Tracking and mean structure of easterly waves over the Intra-Americas Sea. *J. Climate*, **23**, 4823–4840, doi:10.1175/2010JCLI3223.1.

Song, F., and T. Zhou, 2014: Interannual variability of East Asian summer monsoon simulated by CMIP3 and CMIP5 AGCMs: Skill dependence on Indian Ocean–western Pacific anticyclone teleconnection. *J. Climate*, **27**, 1679–1697, doi:10.1175/JCLI-D-13-00248.1.

Sperber, K. R., H. Annamalai, I.-S. Kang, A. Kitoh, A. Moise, A. Turner, B. Wang, and T. Zhou, 2013: The Asian summer monsoon: An intercomparison of CMIP5 vs. CMIP3 simulations of the late 20th century. *Climate Dyn.*, **41**, 2711–2744, doi:10.1007/s00382-012-1607-6.

Strachan, J., P. L. Vidale, K. Hodges, M. Roberts, and M.-E. Demory, 2013: Investigating global tropical cyclone activity with a hierarchy of AGCMs: The role of model resolution. *J. Climate*, **26**, 133–152, doi:10.1175/JCLI-D-12-00012.1.

Tian, S.-F., and T. Yasunari, 1998: Climatological aspects and mechanism of spring persistent rains over central China. *J. Meteor. Soc. Japan*, **76**, 57–71.

Villarini, G., and R. F. Denniston, 2015: Contribution of tropical cyclones to extreme rainfall in Australia. *Int. J. Climatol.*, **36**, 1019–1025, doi:10.1002/joc.4393.

——, R. Goska, J. A. Smith, and G. A. Vecchi, 2014: North Atlantic tropical cyclones and U.S. flooding. *Bull. Amer. Meteor. Soc.*, **95**, 1381–1388, doi:10.1175/BAMS-D-13-00060.1.

Wang, B., and J. C. L. Chan, 2002: How strong ENSO events affect tropical storm activity over the western North Pacific. *J. Climate*, **15**, 1643–1658, doi:10.1175/1520-0442(2002)015<1643:HSEEAT>2.0.CO;2.

Wang, S.-Y., and T.-C. Chen, 2008: Measuring East Asian summer monsoon rainfall contributions by different weather systems over Taiwan. *J. Appl. Meteor. Climatol.*, **47**, 2068–2080, doi:10.1175/2007JAMC1821.1.

Wu, Y., S. Wu, and P. Zhai, 2007: The impact of tropical cyclones on Hainan Island's extreme and total precipitation. *Int. J. Climatol.*, **27**, 1059–1064, doi:10.1002/joc.1464.

Xu, G., T. J. Osborn, and A. J. Matthews, 2016: Moisture transport by Atlantic tropical cyclones onto the North American continent. *Climate Dyn.*, 1–22, doi:10.1007/s00382-016-3257-6.